RECENT SECONDARY ELECTRON MODELING AT PRINCETON PLASMA PHYSICS LABORATORY

C. Swanson*, Princeton Satellite Systems, Plainsboro, New Jersey 08536, USA
I. D. Kaganovich†, Princeton Plasma Physics Laboratory, Princeton, New Jersey 08543, USA

ABSTRACT

Over the past 5 years, researchers at Princeton Plasma Physics Laboratory (PPPL) have been engaged in research to theoretically characterize Secondary Electron Emission (SEE) from complex surfaces. We have used both a Monte Carlo numerical method and an analytic integral model to study the phenomenon. We have studied the specific shapes of velvet, foam, and a feather-like fractal surface using these methods, including parametric dependence (aspect ratio, packing density, angle of incidence). We have found that the Secondary Electron Yield (SEY) of a velvet surface can be significantly smaller ($< 10\%$) than a flat surface, but only for electrons which are normally incident. We have found that the SEY of foam surfaces is much more isotropic with respect to angle of incidence, but that the minimum SEY does not approach that of velvet ($\sim 30\%$). Using the understanding gleaned from analysis of velvet, we proposed a primary velvet with a smaller secondary velvet grown onto it, which we called "feathered" because of its resemblance to down feathers. We have found that a feathered surface exhibits isotropic *and* dramatic SEY reduction.

INTRODUCTION

The interest in Secondary Electron Emission (SEE) at Princeton Plasma Physics Laboratory (PPPL) initially resulted from research into Hall Thrusters. Materials with low Secondary Electron Yield (SEY) were considered a way to reduce near-wall conductivity and to increase the potential profile favourably [15–17]. More broadly, the interest at PPPL is from the effect of SEE on plasma, such as its critical role in maintaining a DC discharge, [11] determining the potential in sheaths, [4] and causing plasma instabilities [19, 25]. The SEY of the Tungsten divertor in the ITER tokamak experiment is expected to be near unity [7, 28].

That said, we are aware of those non-plasma applications which are known to be sensitive to SEE, like accelerators [32] and RF amplifiers [26].

The technique of reducing SEY through the geometry of a surface was mostly confined to regular grooves until this decade [14, 20, 29]. Carbon velvets were early contenders for a surface, receiving both theoretical and experimental attention, both at PPPL and elsewhere [1, 10, 13, 21]. Foams, of the kind that are spontaneously generated when Helium plasma is incident on Tungsten, [28] are also surfaces of interest both at PPPL and elsewhere [5, 12, 23].

Other common structures under consideration are dendritic structures, [3] micro-pores, [31] and micro-spears and -nodules [6]. These micro-architectured materials may often be grown in-place via chemical processes.

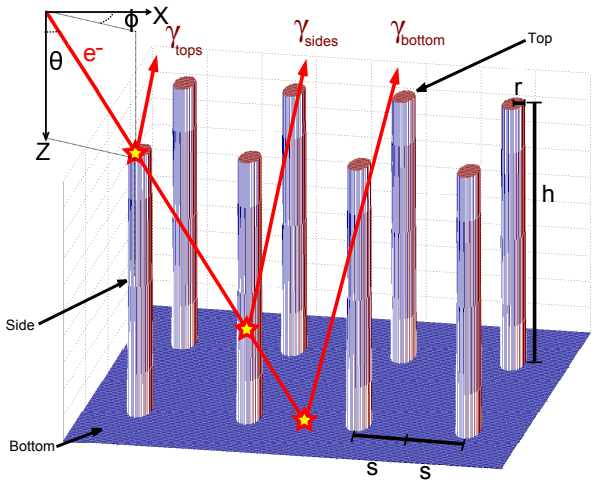

Figure 1: Velvet geometry, including secondary electrons produced on the velvet tops, sides, and bottom substrate

Here at PPPL we attempt via modeling to determine the parametric dependencies of the SEY, for example on aspect ratio, packing density, layer thickness, angle of incidence, etc. Other researchers have also analyzed geometries in this way [27, 30, 31]. Other groups also use a Monte-Carlo tool [2, 8, 9].

THE MECHANISM OF SEY SUPPRESSION

For the mechanism of SEY suppression, see Figure 1. Some incident electrons penetrate deep into the architectured layer. There, they produce secondary electrons. These secondary electrons are typically only a few eV of energy. At this energy, if they hit a surface again, they produce no more secondary electrons and are suppressed.

MONTE CARLO MODEL

The Monte Carlo model we have coded in MATLAB is described in detail by several of our papers [21–23]. It implements geometry as an iso-surface function of space, where $F_{iso}(\vec{x}) > 0$ is outside the geometry and $F_{iso}(\vec{x}) < 0$ is inside the geometry. It initializes 10^5 particles at the top of the simulation and allows them to follow ballistic, straight-line trajectories until they collide with the geometry.

When a collision occurs, the empirical models of Scholtz [18] and Vaughan [24] are used to determine the energy, ve-

* charles.swanson@psatellite.com
† ikaganov@pppl.gov

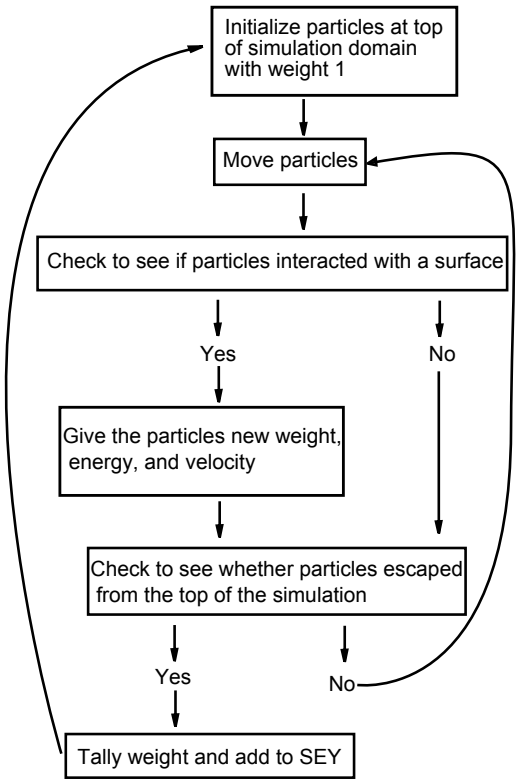

Figure 2: Flowchart of the algorithm used in the Monte Carlo tool

locity angles, and "weight" of the newly emitted secondary electron. Elastically scattered, inelastically scattered ("rediffused"), and "true" secondary electrons are considered. This process is described in more detail in our papers. If a particle escapes the top of the simulation, its weight is counted and it contributes to the SEY. The process is continued until all particles have escaped or their weight diminishes past a threshold. The process of starting with 10^5 particles and changing their weights produces similar ($\sim \sqrt{N}$) counting statistics to the process of starting with some number of particles and having them produce more or fewer daughter particles until 10^5 are reached and counted.

Figure 2 shows a flow chart depicting the algorithm.

VELVET

A velvet is a lattice of long whiskers grown onto a flat substrate. For the Monte Carlo calculation, this lattice was assumed to be rectangular, but real velvets are not. This geometry is depicted in Figure 1. We find that velvet is well suited to suppressing secondary electrons from primary electrons which are normally incident, and find the geometric quantities to optimze for minimum SEY [21].

We characterize the velvet by dimensionless functions of its geometry. From its radius, height, and the areal density of the whiskers (r, h, n), we consider velvets of specific aspect ratio $A = h/r$ and packing density $D = \pi r^2 n$.

We have developed an integral model which treats the probability of an electron-whisker impact as a continuous

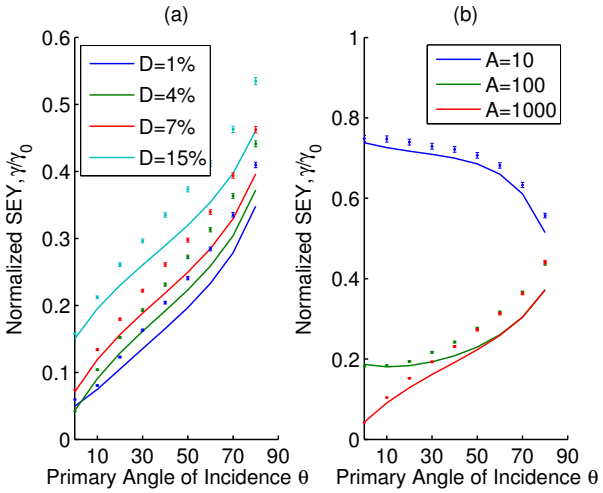

Figure 3: Results of the analyses for velvet: Monte Carlo and integral model. a) $A = 1000$. b) $D = 4\%$

scattering problem, assumes electron trajectories are straight-line between collisions, considers only one generation of secondary electrons, and considers only "true" secondary electrons. The details of this model are given in our velvet paper [21]. Determining the SEY of a single velvet (A, D) requires an integral over the polar velocity angle of the secondary electron population.

The result of the Monte Carlo and integral calculations are depicted in Figure 3. Agreement between the Monte Carlo and integral model can be as poor as 20% discrepancy. This is due to the approximation of the integral model that only one generation of secondaries is produced; in actuality, tertiary electrons from high-energy secondary electrons contribute to the SEY.

Some trends are worth discussing in Figure 3. First, it is apparent that increasing the length of the whiskers, or equivalently the aspect ratio A, decreases the SEY. For SEY reduction from velvet, longer is better.

Second, it is clear that, for the aspect ratios of the most interest to SEY reduction, velvet is best suited to suppressing SEY from primary electrons which are normally incident ($\theta = 0$). Velvet does not suppress SEY from shallowly incident ($\theta \to \pi/2$) electrons to better than 50%.

The integral model reduces to a simple geometric dependence.

$$\gamma_{eff} = \gamma_{flat}[D + (1 - D) f(u, \theta)] \quad (1)$$

where γ_{eff} is the secondary electron yield from the velvet surface, γ_{flat} is the secondary electron yield from a flat surface, D is the packing density, $f(u, \theta)$ is a function which is depicted in Figure 4, θ is the primary angle of incidence, and u is a dimensionless parameter characteristic to the velvet:

$$u = 2rhn = (2/\pi)AD \quad (2)$$

The condition to maximally suppress SEY is found to be

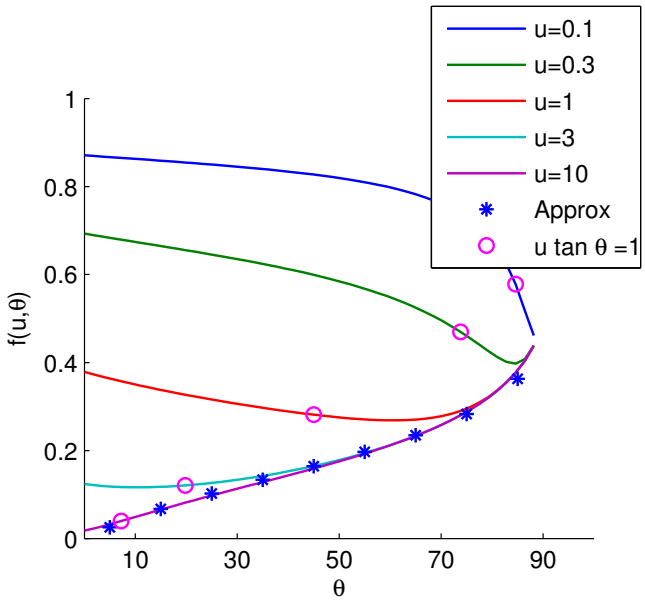

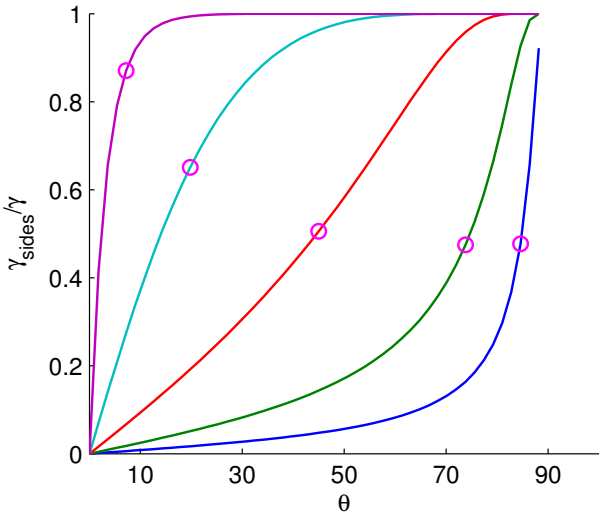

Figure 4: Quantities of interest and location of $u \tan\theta = 1$ point, showing a change in parameter regime for velvet at this point. Top: The dimensionless function $f(u,\theta)$ for several values of u. Bottom: The proportion of SEY which comes from the sides of the whiskers, indicating that $u \tan\theta = 1$ is generally a point at which the SEY behavior becomes dominated by the sides of the whiskers.

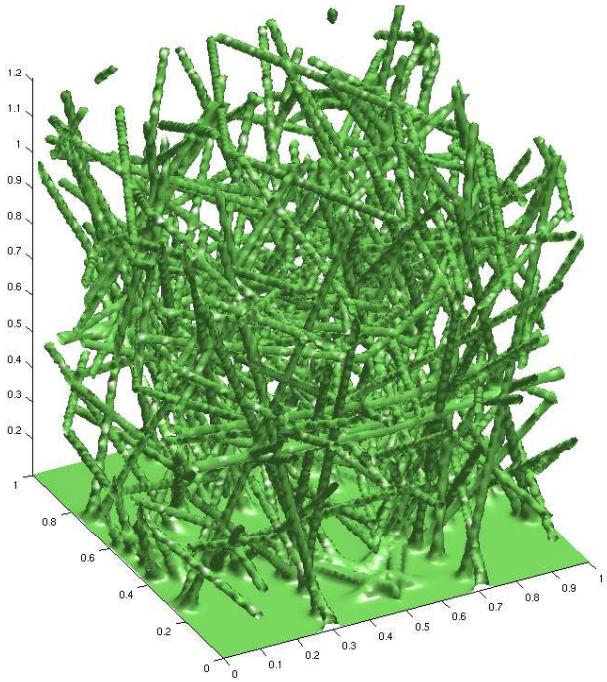

Figure 5: Foam geometry

$$u \to \infty, D \to 0 \tag{3}$$

However even in this limit, there is still finite SEY from all primary angles of incidence except the normal. We have developed an approximate formula for the SEY of velvet in the limit $u \to \infty$:

$$\lim_{u\to\infty} \gamma_{eff} \approx \gamma_{flat} D + \frac{1}{2}\gamma_{flat}(1-D) \times \left[1 - \frac{1}{(1.39\tan\theta + 1)^{0.45}}\right], \tag{4}$$

with average deviation of 0.5% from the exact result. This function is depicted in Fig. 4 (blue symbols).

FOAM

A foam is an array of whiskers which are disordered, and whose axes are aligned isotropically rather than all in the same direction. An example foam geometry can be seen in Figure 5. Foams can occur naturally in plasma applications [28]. We find that foam is much more isotropic with respect to the effect of primary angle of incidence on SEY. However, we also find that the minimum SEY possible from foam is $\sim 0.3\gamma_{flat}$ [23].

The Monte Carlo model was applied to the foam geometry seen in Figure 5. Also, an integral model was formulated with the same approximations as the velvet model: that electrons follow a ballistic, straight-line trajectory between collisions, that collisions follow a continuous-scattering mean-free-path law, that only true secondary electrons are produced, and that only one generation of secondary electrons is produced.

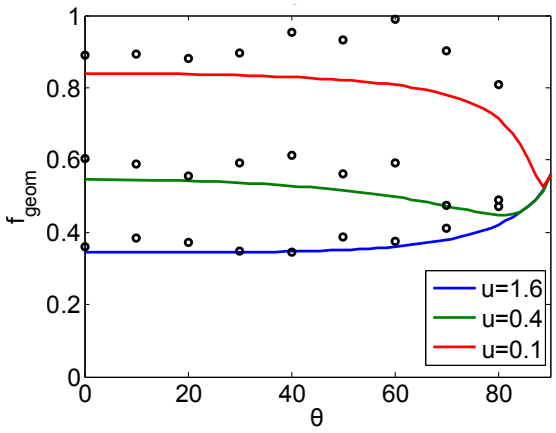

Figure 6: Results of the analyses for foam: Monte Carlo and integral model

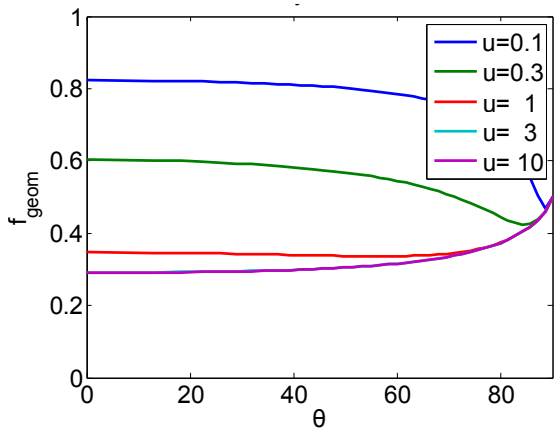

Figure 7: Results of integral foam model, including very high $\bar{u}$ parameter showing asymptote

As in the case of the velvet model, we found helpful dimensionless parameters to be: D, the volume fill fraction of the foam, $A = h/r$, the aspect ratio (ratio of foam layer thickness to whisker radius), and $\bar{u} = AD/2$, a parameter characteristic to the foam. Again like the velvet case, we found that for foam,

$$\gamma_{eff} = \gamma_{flat}[D + (1 - D)f(\bar{u}, \theta)] \quad (5)$$

The comparison between Monte Carlo and integral model is depicted in Figure 6. More values of $f(\bar{u}, \theta)$ appear in Figure 7.

We had initially hoped that foam would have the beneficial properties of velvet without the drawbacks. Indeed, the SEY from foam behaves more isotropically with respect to primary angle of incidence than the SEY from velvet. However, foam has a minimum SEY of around $0.3\gamma_{flat}$, even for the case that $\bar{u} \to \infty, D \to 0$.

We have developed an approximate formula in this limit:

$$\lim_{\bar{u}\to\infty} \gamma_{eff} \approx \gamma_{flat}[D + (1 - D)(C_1 e^{-C_2 \cos\theta} + C_3)] \quad (6)$$

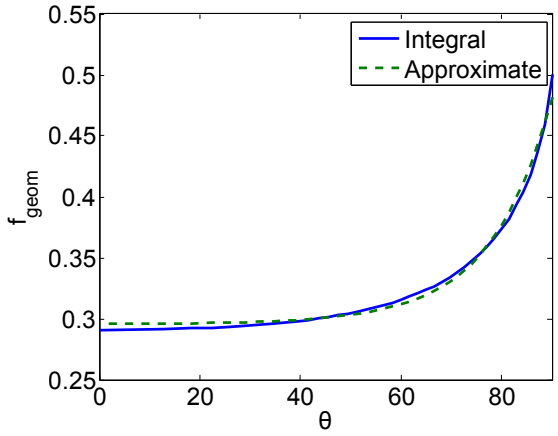

Figure 8: Comparison between approximate foam SEY and full integral model

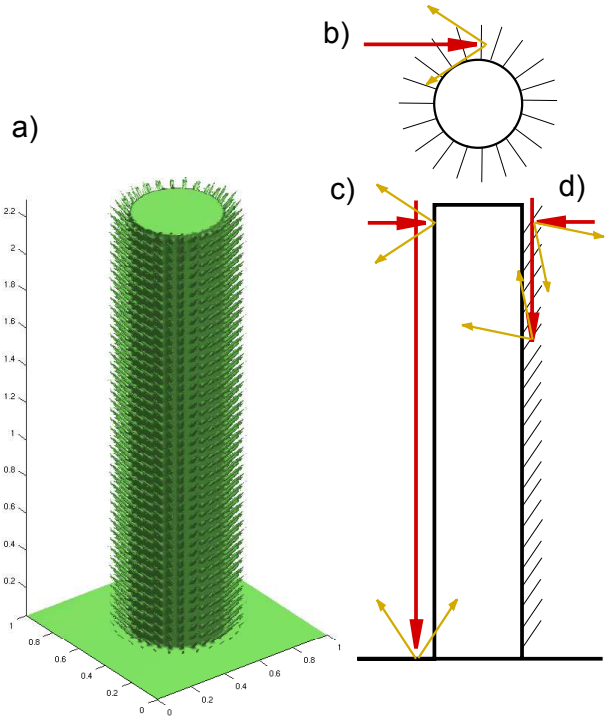

Figure 9: Feather geometry. This depicts $A = 10$, $D = 16\%$ primary and secondary whiskers, which are shorter and fatter than those simulated.

where $C_1 = 0.1887, C_2 = 4.8196, C_3 = 0.2947$. The root-mean-square error of this approximate formula is 0.46%. This fit is depicted in Fig. 8.

FEATHERS

From the lessons of both the velvet and the foam, we attempted to develop a geometry which would overcome the limitations of both. We settled on a feathered geometry, which is a large primary velvet with a small secondary velvet grown onto it. Such a geometry is depicted in Figure 9. The full analysis of this shape can be found in our paper [22].

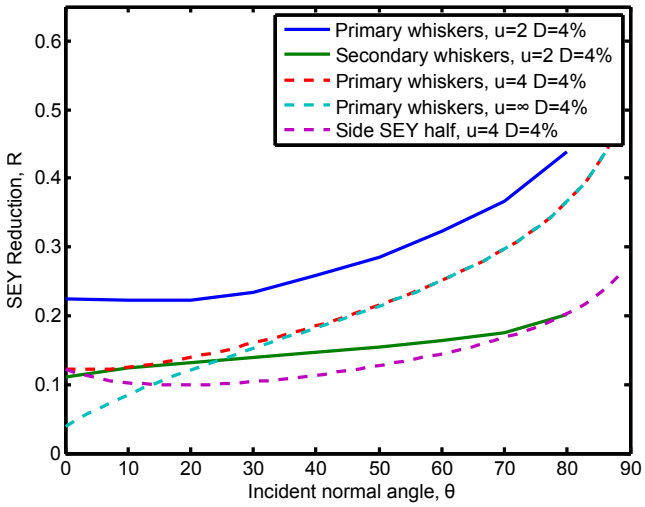

Figure 10: Results of the analyses for feathers: Monte Carlo (solid) and integral (dashed) models

Because of the dynamic range of length scales involved, from the length of the primary whisker to the radius of the secondary whisker, we could not use the Monte Carlo method to simulate the kinds of $A = 1000$ aspect ratios which can be made in the lab. Instead, we considered only a modest $D = 4\%$, $A = 80$ case for both the primary and secondary whiskers. This gives a $u = 2$, by the definition of the velvet u-parameter.

The results of two Monte Carlo and three integral calculations are depicted in Figure 10. "Side SEY half" refers to the case in which we computed the SEY for a velvet of the specified u, D, and reduced the SEY from the whisker sides by one-half.

The green solid line in Figure 10 depicts the feathered case. It lies below the blue solid line, which depicts the primary velvet only. This was expected. Crucially, the green line also lies below the cyan dashed line, which is the integral calculation's result for the SEY of an infinitely long velvet. Thus, feathers are capable of suppressing SEY in the shallow-incidence regime in which velvet can not.

CONCLUSION

PPPL has had a modeling effort over the past 5 years to characterize secondary electron emission (SEE) from complex surfaces. This effort was instigated at least in part by the prospect of using materials with low secondary electron yield (SEY) to improve the performance of Hall thrusters.

We have used a Monte Carlo code and an integral model to examine the SEY properties of velvet, foam, and feathers. Velvet, which is a lattice of whiskers grown onto a flat surface, is found to be suitable for reducing SEY by a large amount ($< 10\%$ the flat SEY), but only for primary electrons which are normally incident. Foam, which is a layer of whiskers which have their axes isotropically aligned, is found to be very isotropic with respect to primary angle of incidence, but suppress SEY by a much less extreme amount (to about $\sim 30\%$ of the flat SEY). We have determined a shape which we calculate to have extreme reduction for normal and shallow incidence; it is a primary velvet with a smaller secondary velvet grown onto the sides of the whiskers.

REFERENCES

[1] L. Aguilera, I. Montero, M. E. Dávila, A. Ruiz, L. Galán, V. Nistor, D. Raboso, J. Palomares, and F. Soria. CuO nanowires for inhibiting secondary electron emission. *Journal of Physics D: Applied Physics*, 46(16):165104, 2013.

[2] A. Alvarado, H.-Y. Chang, W. Nadvornick, N. Ghoniem, and J. Marian. Monte Carlo Raytracing Method for Calculating Secondary Electron Emission from Micro-Architected Surfaces. *arXiv:1806.00205 [cond-mat, physics:physics]*, June 2018. arXiv: 1806.00205.

[3] V. Baglin, J. Bojko, O. Grobner, B. Henrist, N. Hilleret, C. Scheuerlein, and M. Taborelli. The Secondary Electron Yield of Technical Materials and its Variation with Surface Treatments. In *Proceedings of the European Particle Accelerator Conference (EPAC)*, pages 217–221, Austria Center, Vienna Austria, June 2000.

[4] M. D. Campanell, A. V. Khrabrov, and I. D. Kaganovich. Absence of Debye Sheaths due to Secondary Electron Emission. *Physical Review Letters*, 108(25):255001, June 2012.

[5] Cimino. Search for new e-cloud mitigator materials for high intensity particle accelerators (PDF Download Available), 2014.

[6] N. M. Ghoniem, Y. Raitses, R. Shaefer, D. Goebel, I. D. Kaganovich, and B. Williams. Micro-Architectured Materials for Electric Propulsion and Pulsed Power. page 27, 2011.

[7] J. P. Gunn. Evidence for strong secondary electron emission in the tokamak scrape-off layer. *Plasma Physics and Controlled Fusion*, 54(8):085007, 2012.

[8] C. E. Huerta, M. I. Patino, and R. E. Wirz. Secondary electron emission from textured surfaces. *Journal of Physics D: Applied Physics*, 51(14):145202, 2018.

[9] C. E. Huerta and R. E. Wirz. Surface Geometry Effects on Secondary Electron Emission Via Monte Carlo Modeling. In *52nd AIAA/SAE/ASEE Joint Propulsion Conference*. American Institute of Aeronautics and Astronautics, 2016.

[10] C. Jin, A. Ottaviano, and Y. Raitses. Secondary electron emission yield from high aspect ratio carbon velvet surfaces. *Journal of Applied Physics*, 122(17):173301, Nov. 2017.

[11] F. Paschen. Ueber die zum FunkenÃijbergang in Luft, Wasserstoff und KohlensÃđure bei verschiedenen Drucken erforderliche Potentialdifferenz. *Annalen der Physik*, 273(5):69–96, 1889.

[12] M. Patino, Y. Raitses, and R. Wirz. Secondary electron emission from plasma-generated nanostructured tungsten fuzz. *Applied Physics Letters*, 109(20):201602, Nov. 2016.

[13] M. I. Patino and R. E. Wirz. Electron emission from carbon velvet due to incident xenon ions. *Applied Physics Letters*, 113(4):041603, July 2018.

[14] M. Pivi, F. K. King, R. E. Kirby, T. O. Raubenheimer, G. Stupakov, and F. Le Pimpec. Sharp reduction of the secondary electron emission yield from grooved surfaces. *Journal of Applied Physics*, 104(10):104904, Nov. 2008.

[15] Raitses. Electron Emission from Nano- and Micro-Engineered Materials Relevant to Electric Propulsion. 2013.

[16] Y. Raitses, I. D. Kaganovich, A. Khrabrov, D. Sydorenko, N. J. Fisch, and A. Smolyakov. Effect of Secondary Electron Emission on Electron Cross-Field Current in $E times B$ Discharges. *IEEE Transactions on Plasma Science*, 39(4):995–1006, Apr. 2011.

[17] Y. Raitses, D. Staack, A. Dunaevsky, and N. J. Fisch. Operation of a segmented Hall thruster with low-sputtering carbon-velvet electrodes. *Journal of Applied Physics*, 99(3):036103, Feb. 2006.

[18] J. J. Scholtz, D. Dijkkamp, and R. W. A. Schmitz. Secondary electron emission properties. *Philips Journal of Research*, 50(3):375–389, Jan. 1996.

[19] A. I. Smolyakov, W. Frias, I. D. Kaganovich, and Y. Raitses. Sheath-Induced Instabilities in Plasmas with ExB Drift. *Physical Review Letters*, 111(11):115002, Sept. 2013.

[20] G. Stupakov and M. Pivi. Suppression of the effective secondary emission yield for a grooved metal surface. In *Proceedings of the 31st ICFA Advanced Beam Dynamics Workshop on Electron-Cloud Effects*, Napa, CA, USA, 2004.

[21] C. Swanson and I. D. Kaganovich. Modeling of reduced effective secondary electron emission yield from a velvet surface. *Journal of Applied Physics*, 120(21):213302, Dec. 2016.

[22] C. Swanson and I. D. Kaganovich. "Feathered" fractal surfaces to minimize secondary electron emission for a wide range of incident angles. *Journal of Applied Physics*, 122(4):043301, July 2017.

[23] C. Swanson and I. D. Kaganovich. Modeling of reduced secondary electron emission yield from a foam or fuzz surface. *Journal of Applied Physics*, 123(2):023302, Jan. 2018.

[24] D. Sydorenko. *Particle-in-cell simulations of electron dynamics in low pressure discharges with magnetic fields*. PhD thesis, June 2006.

[25] D. Sydorenko, I. Kaganovich, Y. Raitses, and A. Smolyakov. Breakdown of a Space Charge Limited Regime of a Sheath in a Weakly Collisional Plasma Bounded by Walls with Secondary Electron Emission. *Physical Review Letters*, 103(14):145004, Oct. 2009.

[26] J. R. M. Vaughan. Multipactor. *IEEE Transactions on Electron Devices*, 35(7):1172–1180, July 1988.

[27] D. . Wang, Y. . He, M. . Ye, W. . Peng, and W. . Cui. Secondary electron emission characteristics of nanostructured silver surfaces. *Journal of Applied Physics*, 122(15):153302, Oct. 2017.

[28] K. Wang, R. P. Doerner, M. J. Baldwin, F. W. Meyer, M. E. Bannister, A. Darbal, R. Stroud, and C. M. Parish. Morphologies of tungsten nanotendrils grown under helium exposure. *Scientific Reports*, 7:42315, Feb. 2017.

[29] L. Wang, K. Bane, C. Chen, T. Himel, M. Munro, M. Pivi, T. Raubenheimer, and G. Stupakov. Suppression of secondary electron emission using triangular grooved surface in the ILC dipole and wiggler magnets. In *2007 IEEE Particle Accelerator Conference (PAC)*, pages 4234–4236, June 2007.

[30] M. Ye, W. Dan, and H. Yongning. Mechanism of total electron emission yield reduction using a micro-porous surface. *Journal of Applied Physics*, 121(12):124901, Mar. 2017.

[31] M. å. é. Ye, Y. N. è. He, S. G. è. Hu, R. ç. Wang, T. C. è. Hu, J. æ. Yang, and W. Z. å. Cui. Suppression of secondary electron yield by micro-porous array structure. *Journal of Applied Physics*, 113(7):074904, Feb. 2013.

[32] F. Zimmermann. A Simulation study of electron cloud instability and beam induced multipacting in the LHC. Technical Report CERN-LHC-PROJECT-REPORT-095, 1997.